Title:

Rheological characterization of ethylcellulose-based melts for pharmaceutical applications

Authors:

Francesco Baldi[1], Juri Ragnoli[1], Davide Zinesi[1], Fabio Bignotti[1], Francesco Briatico-Vangosa[2], Federica Casati[3], Giulia Loreti[3], Alice Melocchi[3], Lucia Zema[3]*

Affiliations:

[1]Dipartimento di Ingegneria Meccanica e Industriale; Università degli Studi di Brescia; Brescia, Italy

[2]Dipartimento di Chimica, Materiali e Ingegneria Chimica "G. Natta"; Politecnico di Milano; Milano, Italy

[3]Dipartimento di Scienze Farmaceutiche, Sezione di Tecnologia e Legislazione Farmaceutiche "Maria Edvige Sangalli"; Università degli Studi di Milano; Milano, Italy

*Corresponding author: Via G. Colombo 71, I-20133 Milano, Italy;
Telephone: +39-02-503-24654;
e-mail address lucia.zema@unimi.it

Running head:

Rheological characterization of ethylcellulose-based melts

1   **Rheological characterization of ethylcellulose-based melts for pharmaceutical applications**

2

3   Francesco Baldi[1], Juri Ragnoli[1], Davide Zinesi[1], Fabio Bignotti[1], Francesco Briatico-Vangosa[2],

4   Federica Casati[3], Giulia Loreti[3], Alice Melocchi[3], Lucia Zema[3]*

5

6

7   [1]Dipartimento di Ingegneria Meccanica e Industriale; Università degli Studi di Brescia; Brescia,

8   Italy

9   [2]Dipartimento di Chimica, Materiali e Ingegneria Chimica "G. Natta"; Politecnico di Milano;

10   Milano, Italy

11   [3]Dipartimento di Scienze Farmaceutiche, Sezione di Tecnologia e Legislazione Farmaceutiche

12   "Maria Edvige Sangalli"; Università degli Studi di Milano; Milano, Italy

13

14

15

16   *Corresponding author: Via G. Colombo 71, I-20133 Milano, Italy;

17   Telephone: +39-02-503-24654;

18   e-mail address lucia.zema@unimi.it

19

20 **ABSTRACT**

21 Rheological characterization of ethylcellulose (EC)-based melts intended for the production, *via*

22 micro-injection moulding (μIM), of oral capsular devices for prolonged release was carried out.

23 Neat EC, plasticized EC and plasticized EC containing solid particles of a release modifier (filler

24 volume content in the melt around 30%) were examined by capillary and rotational rheometry tests.

25 Two release modifiers, differing in both chemical nature and particle geometry, were investigated.

26 When studied by capillary rheometry, neat EC appeared at process temperatures as a highly viscous

27 melt with a shear-thinning characteristic that progressively diminished as the apparent shear rate

28 increased. Thus, EC as such could not successfully be processed *via* μIM. Plasticization, which

29 induces changes in the material microstructure, enhanced the shear-thinning characteristic of the

30 melt and reduced considerably its elastic properties. Marked wall slip effects were noticed in the

31 capillary flow of the plasticized EC-based melts, with or without release modifier particles. The

32 presence of these particles brought about an increase in viscosity, clearly highlighted by the

33 dynamic experiments at the rotational rheometer. However, it did not impair the material

34 processability. The thermal and rheological study undertaken would turn out a valid guideline for

35 the development of polymeric materials based on pharma-grade polymers with potential for new

36 pharmaceutical applications of μIM.

37

38

39 **Keywords:**   rheology; micro-injection moulding; ethylcellulose; prolonged release

40

INTRODUCTION

Well-established techniques used to process thermoplastic polymers, such as extrusion and injection moulding (IM), have gained over the years considerable interest in the pharmaceutical field, as the number of papers recently published in the scientific literature and of drug products already on the market demonstrate [1-3]. In some applications, considering the weight, dimensions, or dimension tolerances of molded parts, the manufacturing process should be regarded as micro-injection moulding (μIM) rather than IM. Several advantages have been highlighted with respect to the use of IM techniques for pharmaceutical production. These are mainly relevant to the improvement of manufacturing (cost-effective and eco-friendly processes, scalability, suitability for continuous manufacturing) and technological/biopharmaceutical aspects (versatility of the product design, patentability, achievement of solid molecular dispersions/solutions of the active ingredient) [4]. Functional containers, namely gastroresistant and pulsatile-release capsular devices, were lately prepared by μIM starting from polymers with peculiar properties, i.e. solubility at pH>5.5 and erosion/dissolution after swelling, respectively [5-7]. For drug delivery purposes it would also be interesting to develop new polymeric materials intended for the manufacturing by μIM of prolonged-release capsular devices able to slowly release their contents over 12-24 h after oral administration.

On the other hand, limitations may arise from processing pharma-grade materials, in consideration of their rheological/thermomechanical behaviour in the melt state and of their thermal or chemical stability. Moreover, issues may be associated with the active ingredient and the product requirements, such as drug dose, release profile, stability and compliance. In this respect, a rational design of new polymers, or of a new generation of traditional ones with improved thermal properties, has recently been attempted (e.g. Soluplus®, Affinisol™) [8]. Therefore, the need for a thorough understanding of the thermal and rheological properties of pharma-grade polymeric melts and of their impact on both processing conditions and physico-mechanical stability of the final products becomes of utmost importance [9].

67   Based on such premises, the aim of this work was to investigate the rheological behaviour of

68   melts based on ethylcellulose (EC), chosen because it is the most widely employed polymer for the

69   preparation of prolonged drug delivery systems and, moreover, has already been processed in the

70   molten state [10-12]. Both neat and plasticized EC was studied. The plasticizer used was triethyl

71   citrate, the relevant effectiveness as a processing aid for EC-based materials being known from the

72   literature [13]. Besides, as preliminary experiments showed that these materials would fail to yield

73   the pursued release performance, two permeability modifiers (a soluble and a swellable polymer)

74   were added to plasticized EC, based on their ability to create pores in the insoluble capsule wall.

75   The rheological behaviour of these systems, which at processing temperatures consisted of

76   suspensions of solid particles in the plasticized EC melt, was then evaluated. The characterization of

77   the EC-based melts was carried out by both capillary and rotational rheometry. Capillary rheometry

78   was employed to study the processability of the materials in view of their μIM, whereas rotational

79   rheometry experiments were performed to gain a more in-depth understanding of the viscoelastic

80   response.

81

82   **MATERIALS AND METHODS**

83   **Materials**

84   Ethylcellulose, EC (Ethocel™ Std. 100 premium; Dow, United States); triethyl citrate, TEC

85   (Aldrich, Germany); KIR (Kollicoat® IR; BASF, Germany); low-substituted hydroxypropyl

86   cellulose, LHPC (L-HPC NBD 020; Shin-Etsu, Japan).

87

88   **Methods**

89   The following EC-based materials were prepared:

90   - plasticized EC (pEC): EC powder was placed in a mortar and the liquid plasticizer, TEC (20% by

91   weight on the dry polymer), was manually added under hard mixing. The kneaded product was left

92 stand at least 12 h at room temperature (21±5°C, 55±5% RH) before it was ground by means of a

93 blade mill (La moulinette, Moulinex®, SEB, France).

94 - pEC filled with KIR or LHPC particles (pEC/KIR and pEC/LHPC, respectively): KIR powder (d_{50}

95 = 23μm; d_{90} = 55μm) or LHPC powder (d_{50} = 46μm; d_{90} = 129μm), previously desiccated at 40°C in

96 an oven for 24 hours, were mixed in a mortar with pEC in a 3:7 weight ratio. The mixed powders

97 were then stored into bags under vacuum, and characterized within one or two days.

98

99 **Thermal characterization**

100 Thermal analysis on EC and pEC powders was performed on a calorimeter DSC1 STAR by

101 Mettler Toledo (Switzerland), using nitrogen as a purge gas (70 ml/min). Indium was used as a

102 calibration standard. Samples of about 10 mg were heated in aluminum crucibles from 30 to 200°C,

103 maintained at this temperature for 1 min, cooled down to 30°C and reheated up to 200°C. Both

104 heating and cooling steps were carried out at 5°C/min.

105

106 **Capillary rheometry experiments**

107 The tests were performed on a capillary rheometer Rheologic 5000 by Instron CEAST (Italy).

108 In this instrument, the flow rate is imposed by a piston and the extrusion pressure monitored by a

109 melt pressure transducer (data recorded every 0.15 s) placed in the barrel at a distance of 15 mm

110 from the die entry plane**; a schematic of a piston velocity-controlled capillary rheometer is**

111 **reported in Figure 1a**. Preliminary trials were carried out on EC to find suitable test conditions.

112 Long residence times in the melt state promoted chemical degradation processes accompanied by

113 gas formation. As such processes were thermally activated, the maximum test temperature was set

114 at 180°C. 175°C was selected as the reference test temperature; additional tests were carried out at:

115 165, 170 and 180°C on EC; 150, 165 and 170°C on pEC; 150 and 160°C on pEC/KIR and

116 pEC/LHPC. EC could not be examined under 165°C due to the high viscosity of the melt. Flat

117 entrance circular dies made from Vanadis 30^{TM} steel were employed. A die with diameter, d, of 2

118 mm and length to diameter ratio, l/d, of 10 was used with all the materials. Additional dies were

119 employed, at 175°C, for: *i)* the investigation of wall slip effects, on pEC-based systems; *ii)* the

120 determination of die entrance pressure losses, on EC and pEC. More in detail, the additional dies

121 were: with reference to *i)*, a die having d = 1 mm and l/d = 10; with reference to *ii)*, dies having d =

122 2 mm and l/d = 5 and 20, for EC analysis, and a die having d = 1 mm and l/d = 20, for pEC analysis.

123 A barrel with diameter, D, of 15 mm was employed. The apparent shear rate at the die wall, $\dot{\gamma}_{app,w}$,

124 ranged between 17.8 and 560 s^{-1} (with five different levels of $\dot{\gamma}_{app,w}$ per decade, equally spaced on

125 a logarithmic scale, examined from the lowest to the highest). $\dot{\gamma}_{app,w}$ is related to the imposed flow

126 rate, Q, and the die diameter, d, as follows:

127 $$\dot{\gamma}_{app,w} = \frac{32 \cdot Q}{\pi \cdot d^3}$$ (1)

128 Shear rates lower than 17.8 s^{-1} were not considered because time to the attainment of the steady-

129 state would have been too long and degradation phenomena could occur. The tests at 175°C with l/d

130 = 10 and d = 1 mm or 2 mm dies were carried out at least three times to check repeatability.

131   In every test performed, the material, after being loaded into the instrument barrel, was

132 subjected to a pre-heating step over 420 s, under a maximum compacting force of 300 N.

133   All tests with the 2 mm diameter dies were conducted in such a way that the various melts

134 experienced the same pre-fixed flow-history, in consideration of the possibility that the materials

135 underwent residence time-controlled chemical processes while in the melt state. More in detail, the

136 period of time during which a material was subjected to a specific $\dot{\gamma}_{app,w}$ (step) was fixed.

137 Preliminary tests allowed to set the duration of each step (Δt_{step}), chosen in such a way as to

138 guarantee the reaching of flow conditions which could be considered representative of a steady-

139 state for every material, at the different test conditions (temperatures and, for EC, also die lengths).

140 Δt_{step} varied between 12 and 20 s, at the highest and the lowest $\dot{\gamma}_{app,w}$ explored, respectively. With

141   l/d fixed, in a 1 mm die test Δt_{step} had to be higher than in a 2 mm die test, at a given $\dot{\gamma}_{app,w}$, due to

142   the lower absolute time scale of the compression process experienced by the melt in the reservoir

143   (with a 1 mm die the fluid is forced to enter into the capillary with a flow rate that is one eighth of

144   the flow rate used with a 2 mm die).

145

146   **Rotational rheometry experiments**

147   Measurements of the linear viscoelastic properties were carried out using the strain-controlled

148   rheometer ARES G2 by TA Instruments (Unites States). Dynamic frequency sweep experiments

149   under low amplitude (2%) oscillations were carried out with a parallel-plate geometry**; a schematic**

150   **of a strain-controlled rotational rheometer with parallel-plate geometry, for oscillatory shear**

151   **measurement, is reported in Figure 1b**. The diameter of the plates was 25 mm, and the gap was

152   set between 1.3 and 1.8 mm. Preliminary experiments, carried out to identify the adequate test

153   conditions, put in evidence that the results were generally dependent on the overall duration of the

154   test (practically determined by the lower limit of the frequency range explored). This should be

155   attributed to chemical degradation processes, the impact of which is expected to increase with the

156   residence time. Thus, the lower limit of the frequency range explored was set at a relatively high

157   value (10 rad/s). Frequency ranged from 10 to 500 rad/s; ten different frequencies, equally spaced

158   on a logarithmic scale (except 500 rad/s), were examined from the lowest to the highest. The tests

159   were performed on EC at four different temperatures, equally spaced between 160 and 175°C, and

160   on the pEC-based systems, at six different temperatures, equally spaced between 150 and 175°C.

161   Each test was carried out three times at each temperature, to check repeatability.

162   The materials were placed on the rheometer in the form of disks, with diameter of 25 mm,

163   prepared *via* compression moulding on a P200E press by Collin (Germany). During the

164   compression operation, the material was maintained for 280 s under the pressure of 32 bar, at 183°C

165   for EC and 145°C for the pEC-based systems.

166

167 **Scanning Electron Microscopy, SEM, analyses**

168   SEM analyses were carried out both on KIR and LHPC powders, and on the fracture surfaces

169 of the extrudates of the filled pEC-based materials, obtained with the tests at the capillary

170 rheometer.

171   With reference to the analyses on the powders, these were carried out on gold coated powders

172 in a scanning electron microscope (model Zeiss Evo 50 EP) operated in high vacuum mode.

173   With reference to the analyses on the extrudates, for each material examined, a portion of the

174 extruded filament was collected at the exit from the rheometer die during an experiment at 175°C,

175 with the 2 mm die with l/d = 10, at a $\dot{\gamma}_{app,w}$ of 100 s^{-1}. The filament was then broken under liquid

176 nitrogen, in such a way to obtain a fracture surface almost perpendicular to the direction of the flow

177 in the capillary, and the cryo-fractured surface was observed by a scanning electron microscope

178 (model LEO EVO 40). The surface, prior to be analysed, was sputtered with a thin layer of gold.

179

180 **RESULTS AND DISCUSSION**

181 **Thermal response**

182   Figure **2** shows the thermograms of EC and pEC obtained from the first and the second

183 heating scan, respectively. EC exhibits an endothermic peak, close to 190°C, whereas a similar

184 endothermic peak was not observed in pEC heating scans. This endothermic peak, which was

185 observed in both heating scans and thus related to a reversible thermal process, may be ascribed to

186 the melting of high order (crystalline) domains, as suggested by Davidivich-Pinhas et al. [14] with

187 respect to the same EC grade. This would indicate that EC has a semi-crystalline nature that it

188 maintains up to around 190°C. Interestingly, based on the absence of this endothermic peak in the

189 pEC trace, it could be inferred that plasticization with TEC makes the polymer amorphous. The

190 glass transition of EC was clearly detected in the second heating scan only (glass transition

191 temperature, T_g, around 130°C), because the thermal response in the first heating scan was

192 complicated by the very broad peak around 100°C probably relevant to water evaporation. A similar

193 broad peak was found also in the first heating thermogram of pEC, the glass transition of which

194 could not be identified even in the second heating scan.

195

196 **Capillary rheometry experiments**

197 *Extrudate appearance*

198   Following rheometry tests on the EC melt, defect-free (at a macroscopic scale) extrudates

199 were always obtained, except at the highest $\dot{\gamma}_{app,w}$ explored (that is 560 s^{-1}). At this apparent shear

200 rate, the presence of bubbles of size comparable to the extrudate cross-section was noticed,

201 irrespective of the working temperature. The formation of these bubbles, observed for the melt that

202 stayed longer in the reservoir of the rheometer ($\dot{\gamma}_{app,w}$ of 560 s^{-1} corresponds to the highest

203 residence time in the rheometer), might be explained as the consequence of chemical degradation

204 processes [15]. This was supported by results obtained from infrared spectroscopy analyses (data

205 not reported).

206   pEC melt showed two distinct flow regimes within the range of $\dot{\gamma}_{app,w}$ explored in the tests

207 carried out between 165 and 175°C: *i)* a stable steady flow regime, at low levels of $\dot{\gamma}_{app,w}$, and *ii)*

208 an unstable flow regime characterized by the occurrence of melt fracture phenomena, at high levels

209 of $\dot{\gamma}_{app,w}$. The transition from the stable to the unstable regime was detected from the extrudate

210 aspect, whereas no effects on the pressure signal trend occurred. The extrudate from the former

211 regime appeared undistorted, appreciably transparent and with a relatively smooth surface. In the

212 unstable regime, a highly deformed and semi-transparent extrudate, characterized by regular wavy

213 distortions with a typical length around 3 mm, was obtained. Interestingly, the level of $\dot{\gamma}_{app,w}$ at

214 the onset of melt fracture decreased by lowering the test temperature, from 560 s^{-1} at 175°C to 178

215 s^{-1} at 165°C. Extrudates at 150°C were different as compared to those obtained at higher

216   temperatures (distortions were in general more irregular and less marked) and appeared deformed in

217   the whole range of $\dot{\gamma}_{app,w}$ explored.

218   With pEC/KIR and pEC/LHPC melts, at the highest $\dot{\gamma}_{app,w}$ explored (that is 560 s^{-1}), large

219   amplitude fluctuations in the pressure signal were recorded and acceptable steady-state extrusion

220   pressure data could not be measured. Fluctuations could not be ascribed to the occurrence of melt

221   fracture phenomena, since no flow instability could be recognized, and the processes at the basis of

222   their origin are not clear. Due to the presence of the KIR and LHPC particles, the extrudate

223   appeared opaque and with a considerably rough surface. Figures **3**a and b show SEM images of

224   these particles. KIR particles have pseudo-spherical shape and smooth surface, whereas LHPC

225   particles appear as flakes or short fibres with rough surface. Figures **3**c and d show higher

226   magnification SEM images of the fracture surfaces obtained from the pEC/KIR and pEC/LHPC

227   extrudate, respectively. It is worth underlining that both KIR and LHPC particles maintained their

228   solid state at the test temperatures. LHPC particles appear better wetted by the polymer with respect

229   to KIR ones. SEM images of the same surfaces at lower magnification (data not reported) showed

230   that both types of particles are uniformly dispersed within the polymeric matrix.

231

232   ***Apparent viscosity functions***

233   Figures **4**a-d show the steady-state apparent shear viscosity, η_{app}, *vs* apparent shear rate at the

234   die wall, $\dot{\gamma}_{app,w}$, curves obtained for EC and the pEC-based melts at different temperatures and

235   with the die having d = 2 mm and l/d = 10. At a given $\dot{\gamma}_{app,w}$, η_{app} is evaluated as the ratio between

236   the apparent shear stress at the die wall, $\tau_{app,w}$, and $\dot{\gamma}_{app,w}$, with $\tau_{app,w}$ calculated from the steady-

237   state extrusion pressure, ΔP, uncorrected for the die entrance pressure drop, ΔP_{ent}, as:

238   $\tau_{app,w} = \dfrac{\Delta P}{4 \cdot l/d}$ (2)

239 Data at 175°C are the average of three replicated measures (bars in figure represent the standard

240 deviation; when not visible, they are shorter than the symbol height). Working with EC at 165°C,

241 $\dot{\gamma}_{app,w}$ higher than 178 s^{-1} could not be determined since extrusion pressure exceeded the

242 maximum capacity of the pressure transducer (50 MPa). Data indicated with open or thinner

243 symbols and connected by dotted segments should be regarded as critical since melt fracture

244 occurred (for pEC) or acceptable values of steady-state extrusion pressure could not be detected (for

245 EC and filled pEC-based melts, at $\dot{\gamma}_{app,w} = 560$ s^{-1}).

246   The pronounced effect of the test temperature on the viscosity of EC melt is clearly shown in

247 Figure **4**a. Under the assumption that the relationship between ΔP_{ent}, and the true shear stress at the

248 die wall, τ_w, is temperature invariant [16], the time-temperature superposition principle was

249 tentatively applied to the $\tau_{app,w}$ data obtained. Each logarithmic plot of $\tau_{app,w}$ *vs* $\dot{\gamma}_{app,w}$ referred to a

250 specific temperature, T, was horizontally shifted to overlap as much as possible the reference curve

251 at $T_0 = 175$°C. Such a procedure permitted to evaluate, for each temperature, the shift factor, a_T, at

252 constant $\tau_{app,w}$, averaged over the shear stress range explored. Good results with respect to the

253 overlapping were generally obtained, and the shift factor turned out practically independent from

254 the stress level within the whole shear stress range explored. This appears rather surprising taking

255 into account the complex evolving micro-structure of the EC melt.

256   An Arrhenius type dependence on temperature was observed for a_T, and a viscous flow

257 activation energy, $E_{0,s}$, of ≈ 240 kJ/mol was obtained (see [16] for Arrhenius equation) – the

258 subscript "s" is used in $E_{0,s}$ to indicate that the activation energy is derived from steady-state flow

259 properties. By considering that, for an ordinary industrial polymer melt, the viscous flow activation

260 energy derived from fully developed flow tests is of the order of a few tens of kJ/mol and typically

261 keeps smaller than 100 kJ/mol [17,18], the value of $E_{0,s}$ obtained for EC seems very high. The

262 pronounced sensitivity of apparent viscosity to temperature could be related to the thermal response

263 of EC. Due to the tendency to undergo chemical degradation processes at high temperatures, the test

264 temperatures have been kept relatively low, just below the endothermic peak ascribed to the melting

265 of the crystalline domains (see *Thermal response* section). At the test temperatures, EC melt is

266 expected to have a heterogeneous microstructure with high order regions dispersed within an

267 amorphous matrix and, therefore, it can be argued that small temperature variations can induce

268 substantial changes in the material microstructure and in polymer chains mobility. These

269 temperature-induced microstructural modifications are likely to be reflected in the viscous response

270 obtained in the capillary rheometer, which varied widely with temperature. A contribution of

271 thermally activated chemical processes occurring during the rheometry test, which could reduce the

272 length of the polymeric chains and, therefore, the viscosity of the material, could not be ruled out. It

273 is worth noting that the phenomena described above do not explain the "apparent thermorheological

274 simplicity" observed for EC. A comprehensive analysis of the processes that govern the temperature

275 dependence of the viscosity here observed would require an extensive work aimed at studying the

276 chemical-physical processes undergone by EC during a capillary rheometer test, and it could be a

277 matter of further studies.

278   From a_T data, the η_{app} *vs* $\dot{\gamma}_{app,w}$ master curve of EC was constructed at $T_0 = 175°C$ (data at

279 560 s^{-1} have been removed). In Figure **4**a, shifted data-points [($\dot{\gamma}_{app,w} \cdot a_T$; η_{app}/a_T) where a_T is

280 temperature shift factor] are indicated with grey symbols, and dashed line is sketched as a guideline

281 for the eye. The EC melt shows a non-Newtonian behaviour, apparently shear-thinning, but

282 different from that of an ordinary polymer melt. It is characterized by a threshold level of apparent

283 viscosity, $\eta_{app,\infty}$ ($\eta_{app,\infty} \approx 670$ Pa·s), approached at high shear rates. This behaviour recalls that of

284 Bingham fluids [19], even if in this case the existence of a yield stress cannot be firmly stated on the

285 basis of the data obtained. The presence of a threshold at a relatively high level of viscosity clearly

286 indicates that EC can be very hardly processed *via* μIM, at least at process temperatures compatible

287 with its chemical stability. This was confirmed by explorative μIM tests, performed with a μIM

288 press (BabyPlast 6/10P; Cronoplast S.L., Barcelona, Spain) equipped with a disk-shaped screening

289   mould (the details of machine and mould used are reported in [7]). At process temperatures

290   comparable with those used in the capillary rheometer tests, EC could not be processed if un-

291   plasticized.

292   For comparison purposes, the flow curve (master curve at $T_0 = 175°C$) of EC is also reported

293   in Figures **4**b-d relevant to pEC-based melts. From Figure **4**b it can be observed that the

294   plasticization with TEC makes the rheological response of pEC consistent with that of an ordinary

295   polymer melt. The trend of the flow curve does not indicate the existence of a threshold level of

296   apparent viscosity and, at the highest $\dot{\gamma}_{app,w}$ explored, η_{app} of pEC is remarkably lower than that of

297   EC (at 175°C). This suggests for the pEC melt the possibility to be processed *via* μIM. By

298   comparing the flow curves of pEC/KIR and pEC/LHPC, reported in Figures **4**c and d, respectively,

299   with that of pEC, it emerges that the presence of a secondary phase in pEC, either KIR or LHPC

300   particles, promotes an increase in η_{app}, at a given level of $\dot{\gamma}_{app,w}$, without impairing the shear-

301   thinning nature of the response, and therefore the potential for the material to be processed at high

302   shear rates. Also these assumptions were confirmed by preliminary μIM trials performed as above

303   described.

304   As shown in Figures **4**b-d, the test temperature leaves the apparent viscosity function of pEC-

305   based melts practically unchanged. This seems to suggest that the flow of these materials is not

306   governed by the shear viscosity of the melt, and that a more complex flow takes place. Moreover,

307   for unfilled pEC the test temperature was already shown to influence the level of $\dot{\gamma}_{app,w}$ at the

308   onset of melt fracture phenomena (see *Extrudate appearance* section), which are generally related

309   to a complex equilibrium between adhesion and slip of the polymer melt at the wall metal interface

310   [20,21]. As polymer/wall interface processes can play a role in defining the capillary flow of the

311   pEC-based melts, the occurrence of wall slip effects in the capillary flow of these melts was

312   verified.

313   Wall slip effects were studied by the application of the Mooney technique [22]. This approach

314   assumes that the fluid is homogeneous and the slip velocity at the die wall, v_s, is a function of the

315   wall shear stress, τ_w, only. The apparent shear rate at the die wall, $\dot{\gamma}_{app,w}$, which the polymer melt

316   is subjected to during capillary flow at a given τ_w, results from: (i.) a purely viscous bulk

317   contribution, $\dot{\gamma}_{app,w,v}$, that would only depend on the intrinsic behaviour of the material, and (ii.) a

318   wall slip contribution, $\dot{\gamma}_{app,w,s}$, that depends on v_s and die diameter, d, according to Eq. 3:

319    $$\dot{\gamma}_{app,w,s} = \frac{8}{d} \cdot v_s(\tau_w)$$ (3)

320   Tests with different die diameters are carried out and τ_w *vs* $\dot{\gamma}_{app,w}$ curves are obtained. v_s and

321    $\dot{\gamma}_{app,w,v}$ can thus be determined from the slope and the intercept, respectively, of the least square

322   regression straight line that interpolates the $\dot{\gamma}_{app,w}$ *vs* 1/d data (Mooney plot), at a given level of τ_w.

323   In this work, under the assumption that ΔP_{ent}, do not significantly change with the die diameter

324   (supported by the experimental observation that for pEC the levels of ΔP_{ent} measured with the

325   highest contraction ratio, D/d, available are very small, as shown below, in the *Entrance pressure*

326   *losses* section), extrusion pressure data uncorrected for ΔP_{ent} were used, and $\tau_{app,w}$ rather than τ_w

327   data were employed. By considering that slip phenomena can depend in principle also on the

328   extrusion pressure [23], the dies for wall slip analysis were chosen in such a way that similar levels

329   of steady-state extrusion pressure were reached in the experiments. More specifically, data from

330   tests carried out, at 175°C, with dies having different diameter (d = 1 and 2 mm) but same l/d (l/d =

331   10) were used. In Figure **5** the $\tau_{app,w}$ *vs* $\dot{\gamma}_{app,w}$ curves obtained with the two different dies for pEC,

332   pEC/KIR and pEC/LHPC are compared (bars in figure represent the standard deviation; when not

333   visible, they are shorter than the symbol height). The data obtained with the 2 mm die at 560 s^{-1}

334   were not taken into account; for pEC, also the datum obtained with the 1 mm die at 560 s^{-1} was

335   omitted since melt fracture was observed. The curve obtained with the 2 mm die is above the 1 mm

336   die curve over the whole range of $\dot{\gamma}_{app,w}$, independent of the material, thus indicating that slip

337   effects occur. It is worth noting that, contrary to what generally observed for melts based on

338   ordinary polymeric materials exhibiting wall slip in capillary flow [23], at the highest levels of $\tau_{app,w}$

339   (that is of ΔP) the curves obtained with the different dies tend to get closer. For pEC, they even

340   overlap at the highest $\dot{\gamma}_{app,w}$, indicating that, for this material, high levels of ΔP, close to the onset

341   of melt fracture phenomena, lead to slipping suppression. Considering that (i.) $\dot{\gamma}_{app,w}$ data from the

342   curves obtained with the two different die diameters, at a given $\tau_{app,w}$, refer to different residence

343   times in the rheometer (longer for the 1 mm die), and that (ii.) the linearity of the Mooney plot,

344   corresponding to a given $\tau_{app,w}$, could not be proven since only two diameters were used, only slip

345   velocity was determined and referred to as an "apparent slip velocity" (indicated with $v_{s,app}$). In

346   Figure **6**, $v_{s,app}$ is reported as a function of $\tau_{app,w}$ for pEC and the filled pEC-based systems, in a

347   double-logarithmic plot. For pEC, the downward arrow indicates the tendency of slipping

348   phenomena to be suppressed at high levels of $\tau_{app,w}$. As the dependence of $v_{s,app}$ on $\tau_{app,w}$ within the

349   explored range of $\tau_{app,w}$ appeared of power-law-type (linear in a double-logarithmic plot), as for

350   ordinary polymer melts, with particular reference to polyolefins [23,24], data were accordingly

351   fitted. In Figure **6**, power-law fitting curve (dashed line) is traced for each series of data (for pEC

352   the point at $\tau_{app,w} = 76770$ Pa, indicated with an open symbol, was not included in the fitting). The

353   order of magnitude of the slip velocity obtained for the pEC-melts is comparable with that of

354   polyolefin-based melts, but the levels of shear stress at which wall slip phenomena occur are

355   generally lower [23,25]. With respect to the unfilled pEC, the presence of a secondary phase, in

356   pEC/KIR and pEC/LHPC, promotes a decrease in $v_{s,app}$, at a given level of $\tau_{app,w}$, but enlarges the

357    $\tau_{app,w}$ range of slip, allowing high values of $v_{s,app}$ to be reached. This latter effect is due to the

358   different sensitivity of $v_{s,app}$ on $\tau_{app,w}$, exhibited by pEC and the filled pEC-based melts, here

359 represented by the slope of the power-law fitting line (that is 2.0 for pEC, 3.4 and 4.0 for pEC/KIR

360 and pEC/LHPC, respectively). Most of the flow occurs by wall slip, and the slip contribution to the

361 flow rate decreases by increasing the shear stress level; at the lowest level of $\tau_{app,w}$, for the capillary

362 with the highest surface/volume ratio (that is the 1 mm die), it is approximately the 90, 80 and 70%

363 of the imposed flow rate for pEC, pEC/KIR and pEC/LHPC melt, respectively. It can be thought

364 that the pronounced wall slip effects of pEC-based melts are due to the presence of the plasticizer,

365 TEC, which, during the capillary flow, could migrate at the die wall. This hypothesis should be

366 confirmed with specific analyses, which could be a matter of further studies.

367

368 ***Entrance pressure losses***

369   Figures **7**a and b show Bagley plots constructed from the steady-state extrusion pressure, ΔP,

370 data measured at various $\dot{\gamma}_{app,w}$, at 175°C, for EC and pEC, respectively; for EC, ΔP data were

371 measured in tests carried out with dies having diameter of 2 mm (data at 560 s^{-1} were not included

372 in the analysis) whereas, for pEC, in tests with 1 mm dies. At l/d = 10, each datum is the average of

373 three values measured in replicated experiments (standard deviation bars indicated).

374   In Bagley plot, the experimental (l/d; ΔP) data at a given $\dot{\gamma}_{app,w}$ typically lie on a straight

375 line, and ΔP_{ent} value is determined by extrapolating to zero the least square regression line that

376 interpolates them. From Figure **7**a, it clearly emerges that, for EC, at each level of $\dot{\gamma}_{app,w}$ explored,

377 the dependence of ΔP on the die length to diameter ratio, l/d, is not linear. This curvature of the

378 Bagley plots cannot be related to the effect of pressure on viscosity, nor to slipping phenomena,

379 since these factors would induce an upward shift of curves [23]; it rather might be ascribed, at least

380 for the highest levels of $\dot{\gamma}_{app,w}$, to viscous heating effects, mainly occurring in the longest die (that

381 is the die with l = 40 mm), where they are expected to be more marked [26,27]. In support of this

382 discussion is the observation that EC viscosity is very sensitive to temperature, and a small

383   temperature increase produced by viscous heating can give rise to a pronounced decrease in

384   viscosity (and therefore in ΔP). In accordance with these results, for the determination of ΔP_{ent} of

385   EC, only data obtained with the two shorter dies (with $l/d = 5$ and 10), and indicated in Figure **7**a

386   wih full symbols, were used.

387   For the pEC melt, too small ΔP_{ent} values were obtained by applying the Bagley procedure to

388   data from tests performed with 2 mm dies. When very small, ΔP_{ent} values can turn out comparable

389   with the statistical error induced by the extrapolation procedure, thus becoming not reliable.

390   Therefore, it is necessary to resort to a test flow geometry that could induce higher level of ΔP_{ent} to

391   be reached. By considering that at a given $\dot{\gamma}_{app,w}$, the higher the reservoir to die diameter ratio,

392   D/d, the higher is ΔP_{ent} (with D fixed) [28], 1 mm dies were used for ΔP_{ent} evaluation, and more

393   reliable ΔP_{ent} data could be obtained except for the lowest $\dot{\gamma}_{app,w}$. In consideration of the fact that

394   pEC shows wall slip phenomena that can be pressure dependent, for the determination of ΔP_{ent} only

395   data obtained with the two shortest dies available (with $l/d = 10$ and 20) were used (Figure **7**b).

396   For both EC and pEC, at each $\dot{\gamma}_{app,w}$ examined, the value of ΔP_{ent} was determined as the

397   intercept of the straight line traced on the two (l/d; ΔP) valid points (dashed lines in Figures **7**a and

398   b), and, in turn, the true shear stress at the die wall, τ_w, was evaluated. Figure **7** clearly shows that

399   the levels of ΔP_{ent} of EC are considerably higher than those of pEC (for EC, at 316 s^{-1}, ΔP_{ent} is

400   higher than 5 MPa, whereas for pEC, at 560 s^{-1} it does not even reach 1 MPa). In Figure **8**, the ratio

401   between ΔP_{ent} and τ_w is plotted as a function of $\dot{\gamma}_{app,w}$, for both EC and pEC, and power-law fitting

402   curve (dashed line) is traced for each series of data. It clearly emerges that, in the whole range of

403    $\dot{\gamma}_{app,w}$, the level of $\Delta P_{ent}/\tau_w$ obtained for EC is largely higher than that obtained for pEC. By

404   considering that, quoting Jerman and Baird [29], "values of $\Delta P_{ent}/\tau_w$ are thought to represent the

405   elasticity of a polymer melt", this result indicates that plasticization with TEC considerably reduces

406   the elastic character of EC in the melt state. This is further confirmed by the swell behaviour

407   exhibited by the two extrudates: the diameter of the EC extrudate (evaluated after material

408   solidification on samples obtained from tests carried out at 175°C, with the 2 mm die with l/d = 10)

409   was larger than that of the pEC one. The difference between the two materials increased by

410   increasing the level of $\dot{\gamma}_{app,w}$ undergone by the melt in the capillary flow (at 316 s^{-1}, the diameter

411   of EC extrudate was nearly twice that of pEC). The pronounced elastic character exhibited by the

412   EC melt is probably another reflection, at a macroscopic scale, of its peculiar microstructure.

413

414   **Rotational rheometry experiments**

415   Figures **9**a and b show the absolute value of the complex viscosity, $|\eta^*|$, and the dynamic

416   storage modulus, G', *vs* frequency, ω, master curves of the various materials, constructed from the

417   data obtained at the various temperatures examined (reference temperature, $T_0 = 175$°C). Each

418   datum reported in the graphs is the average of three values measured in replicated experiments (bars

419   representing the standard deviation are not reported in the graphs as they were generally shorter

420   than the symbol height). Differently from that observed with the capillary rheometer tests, at the

421   rotational rheometer also for the pEC-based melts a clear effect of temperature was observed. This

422   is probably due to the fact that the shear stress levels reached in these latter tests, remarkably lower

423   than those reached in the capillary experiments, are insufficient to promote slip phenomena. The

424   successful attainment of a master curve for each system examined by shifting the rheological data

425   with respect to frequency, on the basis of the temperature shift factors, a_T, demonstrates the validity

426   of the time-temperature superposition principle [already demonstrated for the EC melt by referring

427   to the capillary rheometer results (see *Capillary rheometry experiments, Apparent viscosity*

428   *functions* section)]. An Arrhenius type dependence on temperature was observed for a_T, and a flow

429   activation energy, $E_{0,d}$, was obtained for each melt – the subscript "d" is used in $E_{0,d}$ to indicate that

430   this flow activation energy is obtained from flow properties measured in dynamic tests. $E_{0,d}$ values

431   are reported in Table I. For the EC melt, an appreciable difference between the flow activation

432   energy calculated from capillary and rotational rhometer tests was obtained. This difference should

433   be related to the different mechanical histories experienced by the polymer melt in the two

434   rheometers. $E_{0,d}$ of pEC is largely lower than that of EC. In consideration of the differences between

435   the microstructures of these two melts (see *Thermal response* section), this result seems to support

436   the idea that the high sensitivity to temperature exhibited by EC might be ascribed to the presence

437   of high order domains in its melt microstructure, that were not found in the pEC melt. Finally, the

438   incorporation of either KIR or LHPC particles in the pEC induces an increase in $E_{0,d}$.

439   From Figure **9** it emerges that the viscoelastic behaviour of the pEC-based melts is that

440   typical of homogeneous polymer melts [30]. With respect to the neat pEC melt, the presence of a

441   secondary phase in pEC/KIR and pEC/LHPC melts induces a significant increase in both G' and

442   $|\eta^*|$, within the explored range of frequency. This result is in agreement with the effects reported in

443   literature for polymer melts filled with rigid particles [19,31], indicating that KIR and LHPC

444   particles enhance the capacity of the pEC melts to store elastic energy and dissipate mechanical

445   energy. Interestingly, LHPC particles appear the most effective in promoting an increase in both

446   dynamic properties. By considering for pEC melt a density of 1.01 g/cm^3 (measured by melt flow

447   rate tests carried out by a Modular Melt Flow Indexer by Ceast-Instron, at 170°C, with an extruding

448   mass of 10 kg, according to ISO 1133-1:2011), and for KIR and LHPC particles density values of

449   0.94 and 1.29 g/cm^3, respectively (evaluated from volume and mass data collected from three

450   compacts prepared by means of a hydraulic press equipped with flat punches), 32 and 25% of actual

451   filler volume contents in pEC/KIR and pEC/LHPC melts were estimated. This result indicates that

452   the higher effectiveness exhibited by LHPC particles cannot be ascribed to a higher volume content

453   of rigid particles in the melt, but it is intrinsically associated with the nature of these particles,

454   which differ from those of KIR in geometry, surface roughness and chemical composition.

455   Interestingly, by considering that LHPC particles (i.) promote an increase in G' and $|\eta^*|$ that is

456   practically independent of the frequency, and (ii.) leave the out-of-phase angle, δ (tan[δ]=G''/G'),

457   practically unchanged (data of δ not shown here), with respect to the unfilled melt, the viscoelastic

458   response of pEC/LHPC seems to be governed by the matrix. By contrast, for pEC/KIR melt, the

459   frequency dependence of the dynamic properties and the values of the out-of-phase angle obtained,

460   which are different from those of the matrix, suggest that KIR particles embedded in the polymer

461   melt actively contribute to its viscoelastic response.

462   The viscoelastic behaviour of the EC melt differs considerably from that of the pEC-based

463   melts and this might be ascribed to its particular microstructure. In Figure **10**, the shear viscosity, η,

464   obtained from capillary rheometer tests is compared with the complex viscosity, $|\eta^*|$, obtained from

465   rotational rheometer tests (viscosity data measured at 175°C). η data are determined from data of

466   true shear stress (corrected for ΔP_{ent}), τ_w, and true shear rate (calculated according to the

467   Rabinowitsch–Weissenberg method [30]), $\dot{\gamma}$, both evaluated at the die wall, and are plotted as a

468   function of $\dot{\gamma}$. It emerges that the Cox-Merz rule [30], according to which an approximate

469   agreement exists between $|\eta^*(\omega)|$ and the steady-state shear viscosity, $\eta(\dot{\gamma})$, if the angular

470   frequency, ω in [rad/s], is set equal to the shear rate, $\dot{\gamma}$ in [s^{-1}], is not verified. In fact, within the

471   range of $\dot{\gamma}$ explored, the value of $|\eta^*|$ is roughly 2.5 times that of η. Even by replotting the complex

472   viscosity data as a function of the maximum (or "effective") shear rate experienced in the dynamic

473   tests, that is ω multiplied by the amplitude of the oscillation (0.02 in these experiments), as

474   proposed for filled melts by Doraiswamy et al. [32], steady-state and complex viscosity data do not

475   overlap. The mechanical history experienced by the melt in the two types of rheometer is different

476   with respect to: (i.) the type of flow (a steady-state pressure-induced shear flow in the capillary

477   rheometer, and a dynamic drag-induced shear flow under low amplitude oscillation in the rotational

478   rheometer); (ii.) the residence time (a capillary rheometer test is roughly two times longer than a

479   rotational rheometer test). In addition, the material tested at the rotational rheometer underwent a

480   compression moulding operation prior to be tested. These differences are likely to be at the basis of

481   the differences between viscosity and flow activation energy data obtained with the two types of

482   test. More specifically, with reference to the viscosity, it is reasonable to think that data coming

483   from the capillary rheometer refer to a melt characterized by a higher degree of microstructural

484   orientation. In spite of the difference between the values of η and $|\eta^*|$, the dependence on the time-

485   variable (either $\dot{\gamma}$ or ω) observed for the two different sets of viscosity data is similar, and may

486   suggest that the shear-thinning characteristic of the melt is being progressively reduced as $\dot{\gamma}$ (or ω)

487   increases. Interestingly, the trend of the viscosity function obtained from the rotational rheometer

488   tests does not suggest the existence of a threshold viscosity for EC melt. This result seems to

489   indicate that the threshold noted for the apparent viscosity ($\eta_{app,\infty}$ in Figure **4**a), coming from

490   capillary rheometer tests, originates in part from the high levels of die entrance pressure losses that

491   this melt exhibits at high $\dot{\gamma}_{app,w}$ (it is worth recalling that η_{app} data were evaluated from data of

492   apparent shear stress, $\tau_{app,w}$, uncorrected for ΔP_{ent}).

493

494   **CONCLUSION**

495   In this work, a rheological characterization of ethylcellulose (EC)-based melts intended to be

496   used for the production *via* μIM of prolonged-release capsular devices was carried out. Neat EC,

497   EC plasticized with TEC (pEC), and pEC containing particles of either a water soluble polymer

498   (KIR) or a hydrophilic swellable polymer (LHPC), added to enhance the permeability of the EC-

499   based materials in view of their final use, were examined by both capillary and rotational rheometry

500   tests.

501   Capillary rheometry tests showed that this peculiar melt, which is expected to have a

502   heterogeneous microstructure with high order regions dispersed within an amorphous matrix,

503   exhibits a non-Newtonian, apparently shear-thinning behaviour characterized by a threshold in the

504   steady-state apparent shear viscosity, η_{app}, approached at high flow rates. The existence of this η_{app}

505   threshold indicates that neat EC cannot be practically processed *via* μIM. From both capillary and

506   rotational rheometry experiments EC melt shows a very high sensitivity of viscosity to temperature.

507   Capillary rheometry tests suggest that plasticization with TEC makes EC (pEC) processable

508   *via* μIM. For the pEC melt, which has a homogeneous amorphous structure, the threshold in the η_{app}

509   was not observed, and a η_{app} function consistent with that of an ordinary polymer melt was

510   obtained. Plasticization with TEC considerably reduces the elastic character of EC, and fosters the

511   occurrence of pronounced wall slip phenomena in the capillary flow. Also for the pEC melts filled

512   with the permeability modifiers, either KIR or LHPC particles (filler volume content around 30%),

513   most of the capillary flow occurs by wall slip. The presence of these particles in the pEC melt

514   induces an increase in η_{app}, which however does not compromise the material shear-thinning

515   behaviour, and therefore its processability. Rotational rheometry experiments clearly indicate that,

516   in the frequency range explored, both LHPC and KIR particles induce an increase in both the

517   complex viscosity, $|\eta^*|$, and the dynamic storage modulus, G', with LHPC particles being the most

518   effective at promoting this increase. KIR particles seem to actively contribute to the frequency

519   dependency of the dynamic properties, whereas the frequency response of the pEC melt filled with

520   LHPC particles seems to be governed by the matrix.

521   The study performed on EC turned out to be a valuable guideline for the development of

522   polymeric materials with potential for new pharmaceutical applications of μIM.

523

531

532

REFERENCES

[1] Lang B, McGinity JW, Williams III RO. Hot-melt extrusion – basic principles and pharmaceutical applications. Drug Dev Ind Pharm. 2014;40:1133-1155.

[2] Repka MA, Shah S, Lu J, Maddineni S, Morott J, Patwardhan K, Mohammed NN. Melt extrusion: process to product. Expert Opin Drug Deliv. 2012;9:105-125.

[3] Zema L, Loreti G, Melocchi A, Maroni A, Gazzaniga A. Injection molding and its application to drug delivery. J Control Release. 2012;159:324-331.

[4] Shah S, Maddineni S, Lu J, Repka MA. Melt extrusion with poorly soluble drugs. Int J Pharm. 2013;453:233-252.

[5] Zema L, Loreti G, Melocchi A, Maroni A, Palugan L, Gazzaniga A. Gastroresistant capsular device prepared by injection molding. Int J Pharm. 2013;440:264-272.

[6] Gazzaniga A, Cerea M, Cozzi A, Foppoli A, Maroni A, Zema L. A novel injection-molded capsular device for oral pulsatile delivery based on swellable/erodible polymers. AAPS Pharm Sci Tech. 2011;12:295-303.

[7] Claeys B, De Coen R, De Geest BG, De la Rosa VR, Hoogenboom R, Carleer R, Adriaensens P, Remon JP, Vervaet C. Structural modifications of polymethacrylates: Impact on thermal behavior and release characteristics of glassy solid solutions. Eur J Pharm Biopharm. 2013;85:1206-1214.

[8] Aho J, Boetker JP, Baldursdottir S, Rantanen J. Rheology as a tool for evaluation of melt processability of innovative dosage forms. Int J Pharm. 2015;494:623-642.

559

560 [9] Zema L, Loreti G, Macchi E, Foppoli A, Maroni A, Gazzaniga A. Injection-molded capsular

561 device for oral pulsatile release: development of a novel mold. J Pharm Sci. 2013;102:489-499.

562

563 [10] Quinten T, Gonnissenn Y, Adriaens E, De Beer T, Cnudde V, Masschaele B, Van Hoorebeke

564 L, Siepmann J, Remon JP, Vervaet C. Development of injection moulded matrix tablets based on

565 mixtures of ethylcellulose and lowsubstituted hydroxypropylcellulose. Eur J Pharm Sci.

566 2009;37:207-216.

567

568 [11] Quinten T, De Beer T, Almeida A, Vlassenbroeck J, Van Hoorebeke L, Remon JP, Vervaet C.

569 Development and evaluation of injection-molded sustained-release tablets containing ethylcellulose

570 and polyethylene oxide. Drug Dev Ind Pharm. 2011;37:149-159.

571

572 [12] Bar-Shalom D, Slot L, Wang Lee W, Wilson CG. Development of the Egalet® technology. In:

573 Rathbone MJ, Hadgraft J, Roberts MS, editors. Modified-release drug delivery technology. New

574 York: Marcel Dekker; 2003.

575

576 [13] Maru SM, De Matas M, Kelly A, Paradkar A. Characterization of thermal and rheological

577 properties of zidovidine, lamivudine and plasticizer blends with ethyl cellulose to assess their

578 suitability for hot melt extrusion. Eur J Pharm Sci. 2011;44:471-478.

579

580 [14] Davidivich-Pinhas M, Barbut S, Marangoni AG. Physical structure and thermal behaviour of

581 ehtylcellulose. Cellulose. 2014;21:3243-3255.

582

583 [15] Lai HL, Pitt K, Craig DQM. Characterization of the thermal properties of ethylcellulose using

584 differential scanning and quasi-isothermal calorimetric approaches. Int J Pharm. 2010;386:178-184.

585

586   [16] Laun HM, Schuch H. Transient elongational viscosities and drawability of polymer melts. J

587   Rheol. 1989;33:119-175.

588

589   [17] Laun HM. Orientation effects and rheology of short glass fiber-reinforced thermoplastics.

590   Colloid Polym Sci. 1984;262:257-269.

591

592   [18] Baldi F, Franceschini A, Bignotti F, Tieghi G, Riccò T. Rheological behaviour of nano-

593   composites based on polyamide 6 under shear and elongational flow at high strain rates. Rheol

594   Acta. 2009;48:73-88.

595

596   [19] Larson RG. The Structure and Rheology of Complex Fluids. New York: Oxford University

597   Press; 1999.

598

599   [20] Hatzikiriakos SG, Dealy JM. Role of slip and fracture in the oscillating flow of HDPE in a

600   capillary. J Rheol. 1992;36:845-884.

601

602   [21] Piau J-M, El Kissi N, Toussaint F, Mezghani A. Distortions of polymer melt extrudates and

603   their elimination using slippery surfaces. Rheol Acta. 1995;34:40-57.

604

605   [22] Mooney M. Explicit formulas for slip and fluidity. J Rheol. 1931;2:210-222.

606

607   [23] Hatzikiriakos SG, Dealy JM. Wall slip of molten high density polyethylenes. II. Capillary

608   rheometer studies. J Rheol. 1992;36:703-741.

609

610

611   [24] Laun HM. Capillary rheometry for polymer melts revised. Rheol Acta. 2004;43:509-528.

612

613   [25] Haworth B, Khan SW. Wall slip phenomena in talc-filled polypropylene compounds. J Mater

614   Sci. 2005;40:3325-3337.

615

616   [26] Cox HW, Macosko CW. Viscous dissipation in die flows. AIChE J. 1974;20:785-795.

617

618   [27] Rosenbaum EE, Hatzikiriakos SG. Wall slip in the capillary flow of molten polymers subject

619   to viscous heating. AIChE J. 1997;43:598-608.

620

621   [28] Baldi F, Ragnoli J, Briatico-Vangosa F. Measurement of the high rate flow properties of filled

622   HDPE melts by capillary rheometer: Effects of the test geometry. Polym Test. 2014;37:201-209.

623

624   [29] Jerman RE, Baird DG. Rheological properties of Copolyester Liquid Crystalline Melts. I.

625   Capollary Rheometer. J Rheol. 1981;25:275-292.

626

627   [30] Macosko CW. Rheology: principles, measurements and applications. New York: Wiley-VCH

628   Inc.; 1994.

629

630   [31] Khan SA, Prud'Homme RK. Melt rheology of filled thermoplastics. Rev Chem Eng.

631   1987;4:205-270.

632

633   [32] Doraiswamy D, Mujumdar AN, Tsao I, Beris AN, Danforth SC, Metzner AB. The Cox-Mertz

634   rule extended: A rheological model for concentrated suspensions and other materials with a yeld

635   stress. J Rheol. 1991;35:647-685.

636

637   Dear Editor,

638

639   we would like to thank the Reviewers for appreciating our work and providing helpful

640   comments.

641   Please find below an outline explaining how such comments have been addressed.

642

643   **Reviewer #1**

644   *The current manuscript is a lucid read and clearly explains each phenomenon observed while using*

645   *rotational and capillary rheometry experiments and extending the results and confirming the same*

646   *to understand the processability of the polymers during thermal extrusion. I recommend to accept*

647   *the manuscript in its current form.*

648

649   We kindly thank the reviewer for his comments.

650

651   **Reviewer #2**

652   *Authors are reporting a study of rheological characterization of molten polymer systems using*

653   *capillary and rotational rheometers. It would be helpful for an average reader if authors could add*

654   *a schematic figure comparing the measurement principle and sample placement with these two*

655   *methods.*

656

657   We followed the suggestion of the reviewer by introducing a new Figure 1 in the manuscript

658   showing the measurement principle and sample placement in both capillary and rotational

659   rheometers. The main text of the manuscript has been changed accordingly (in the revised

660   manuscript Figure 1 has been mentioned at lines 110 and 149, and all the other figures have been

661   renumbered).

Table I

Table I – Flow activation energies, $E_{0,d}$, of melts from dynamic tests at the rotational rheometer.

Material	$E_{0,d}$ [kJ/mol]
EC	335
pEC	120
pEC/KIR	140
pEC/LHPC	150

Figure captions

Figure 1 – Schematic of (a) a capillary rheometer (piston velocity-controlled) and (b) a rotational rheometer with parallel-plate geometry (strain-controlled, for oscillatory shear measurement). With reference to (a): v_P, piston velocity; P, resulting pressure in the reservoir. With reference to (b): θ, angular displacement; ω, oscillation frequency; M, resulting torque.

Figure **2** – DSC traces of EC and pEC obtained from the first and the second heating scans (thermograms vertically shifted for clarity).

Figure **3** – SEM images of (a) KIR and (b) LHPC particles, and of cryo-fracture surfaces obtained from the extrudates of (c) pEC/KIR and (d) pEC/LHPC.

Figure **4** – Steady-state apparent shear viscosity, η_{app}, *vs* apparent shear rate at die wall, $\dot{\gamma}_{app,w}$, for (a) EC, (b) pEC, (c) pEC/KIR, (d) pEC/LHPC, from capillary rheometry tests at: 180°C, *circle* (a); 175°C, *square* (a-d); 170°C, *triangle* (a,b); 165°C, *rhomb* (a,b); 160°C, *"×"* (c,d); 150°C, *asterisk* (b-d).

Figure **5** – Apparent shear stress at the die wall, $\tau_{app,w}$, as a function of the apparent shear rate at the die wall, $\dot{\gamma}_{app,w}$, for pEC (*square*), pEC/KIR (*circle*), pEC/LHPC (*triangle*), from capillary rheometry tests at 175°C, with d = 2 mm (full symbols) and d = 1 mm (open symbols).
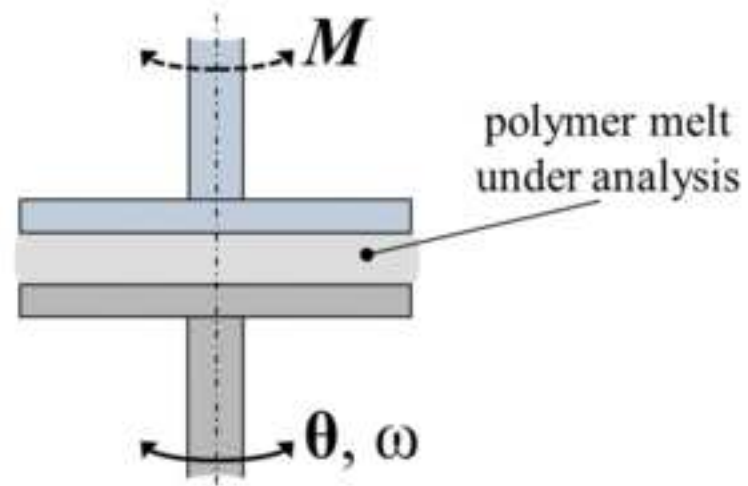
Figure **6** – "Apparent wall slip velocity", $v_{s,app}$, as a function of the apparent shear stress at the die wall, $\tau_{app,w}$, for pEC (*square*), pEC/KIR (*circle*), pEC/LHPC (*triangle*), from capillary rheometry tests at 175°C.
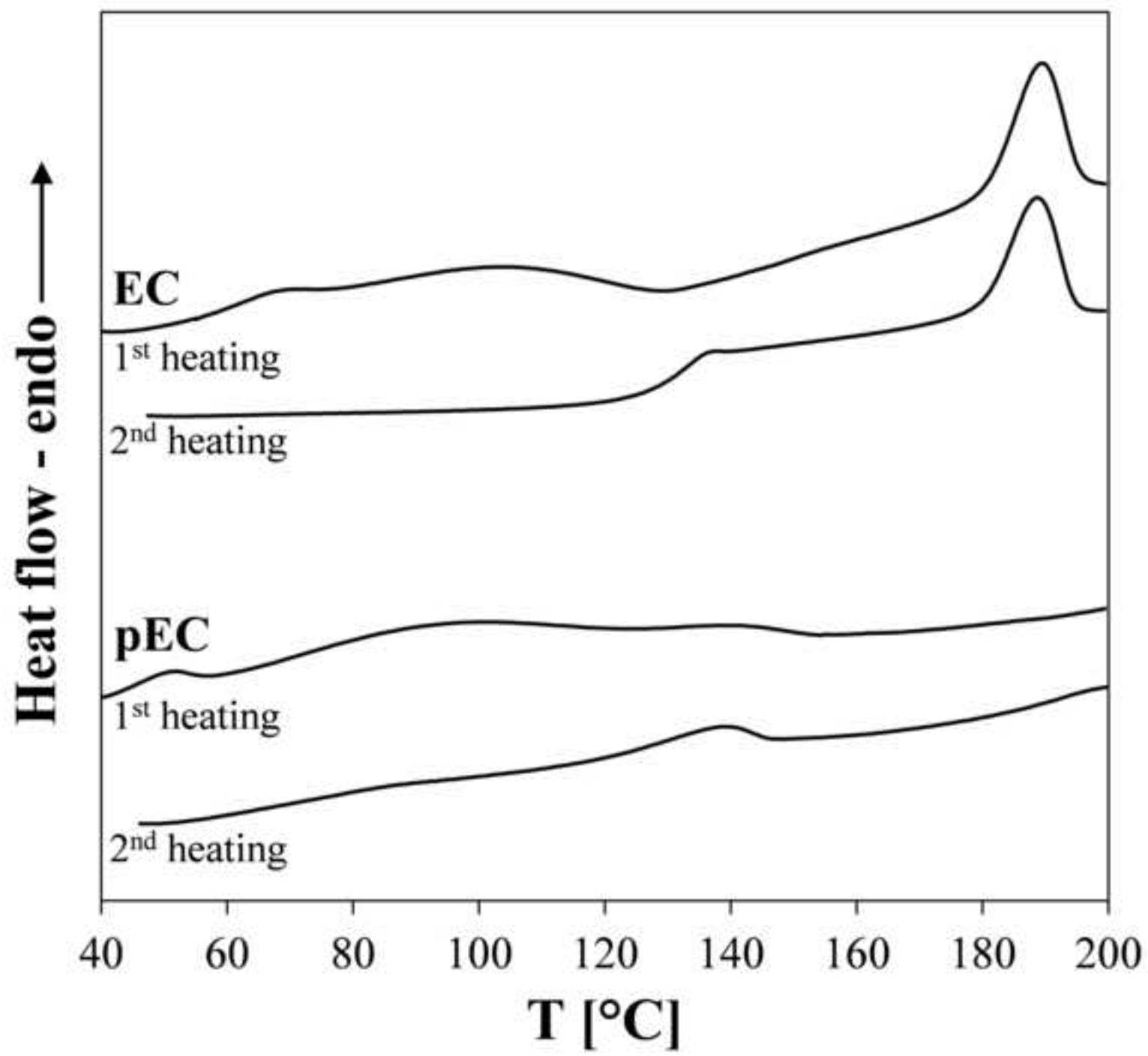
Figure **7** – Bagley plots for (a) EC and (b) pEC, from capillary rheometry tests carried out with dies having d = 2 mm for EC (a) and d = 1 mm for pEC (b), at 175°C. For EC (a), data-points at l/d = 20 (open symbols) not used for ΔP_{ent} determination.
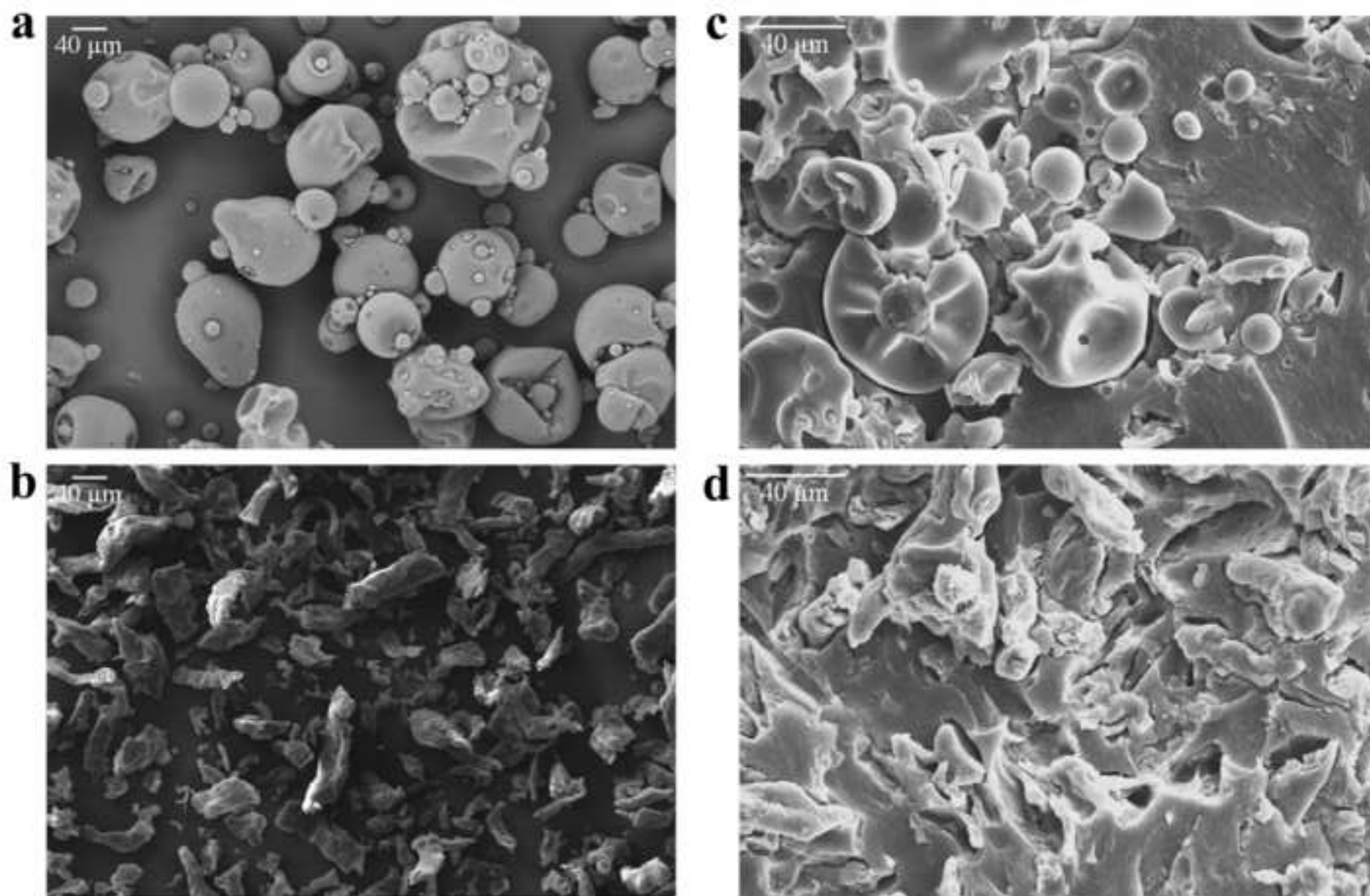
Figure **8** – Ratio between the die entrance pressure drops, ΔP_{ent}, and the true shear stress at the die wall, τ_w, as a function of the apparent shear rate at the die wall, $\dot{\gamma}_{app,w}$, for EC (*rhomb*) and pEC (*square*), from capillary rheometry tests at 175°C.

Figure **9** – (a) Absolute value of the complex viscosity, $|\eta^*|$, and (b) dynamic storage modulus, G', *vs* frequency, ω, master curves (T_0 = 175°C) of EC (*rhomb*), pEC (*square*), pEC/KIR (*circle*) and pEC/LHPC (*triangle*), from rotational rheometry experiments.

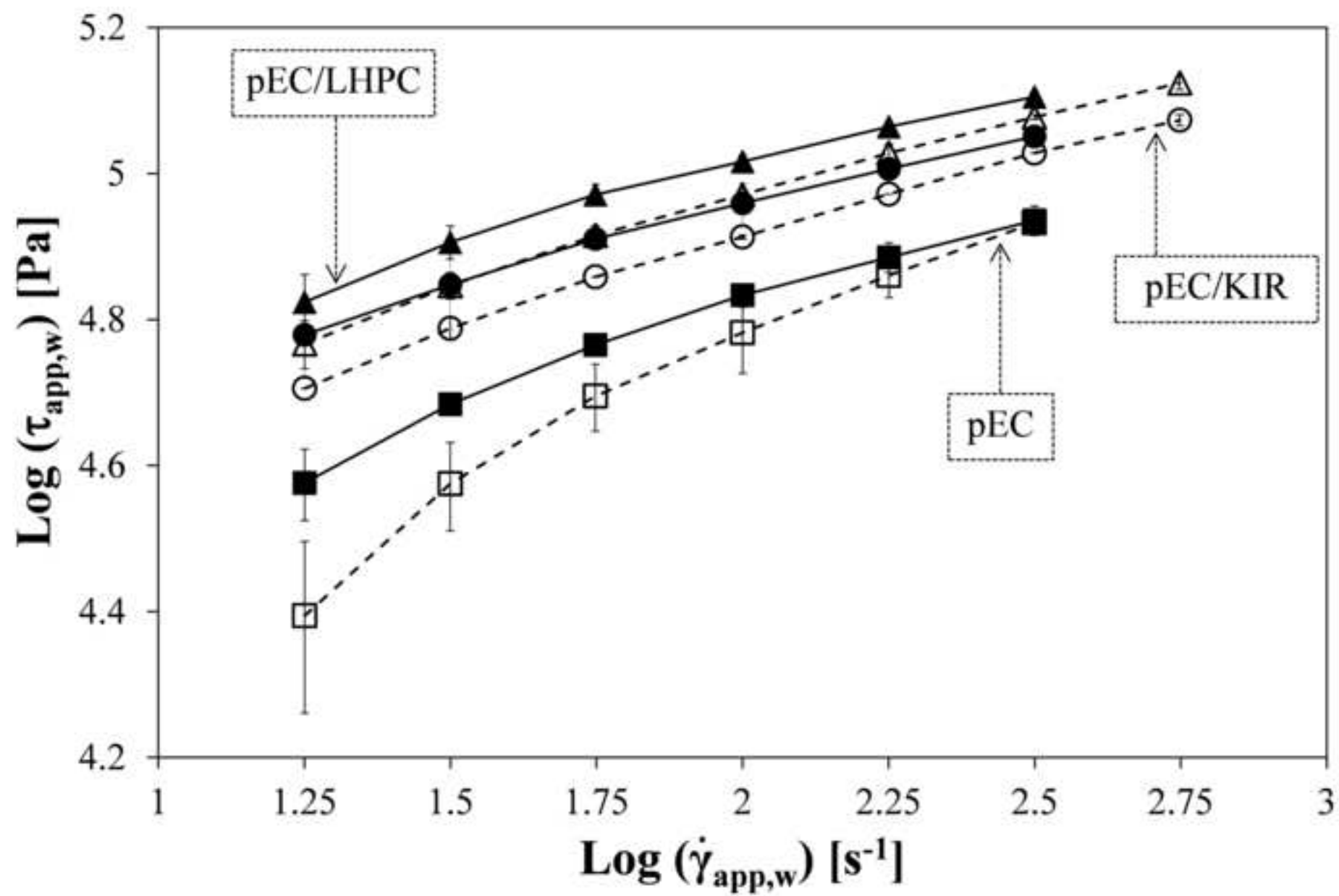Figure **10** – Steady-state shear viscosity, η, *vs* shear rate (at the die wall), $\dot{\gamma}$, curve from capillary rheometry tests (open symbols) compared with the absolute value of the complex viscosity, $|\eta^*|$, *vs* frequency, ω, master curve from rotational rheometry tests (full symbols) for EC, at 175°C.
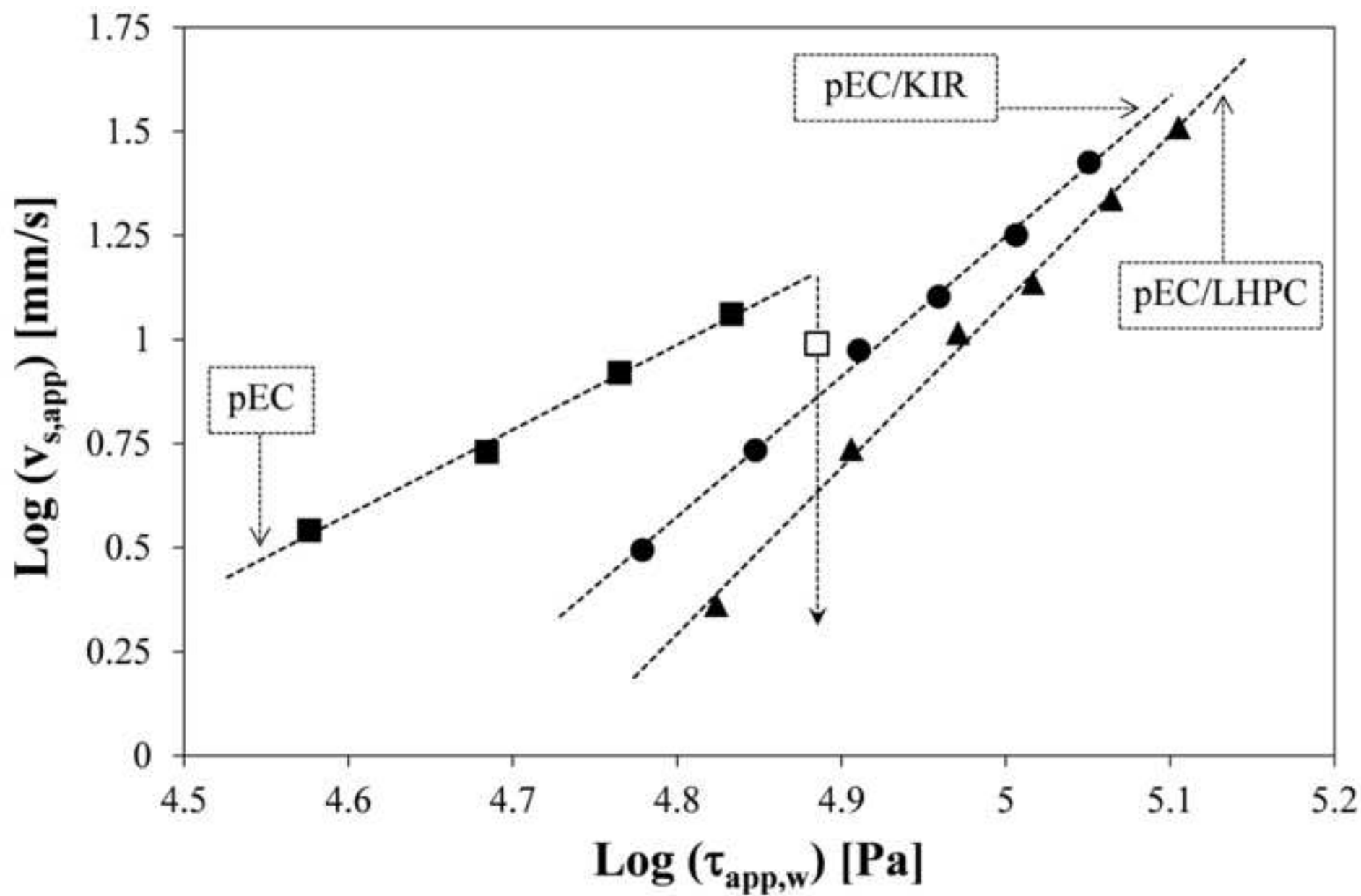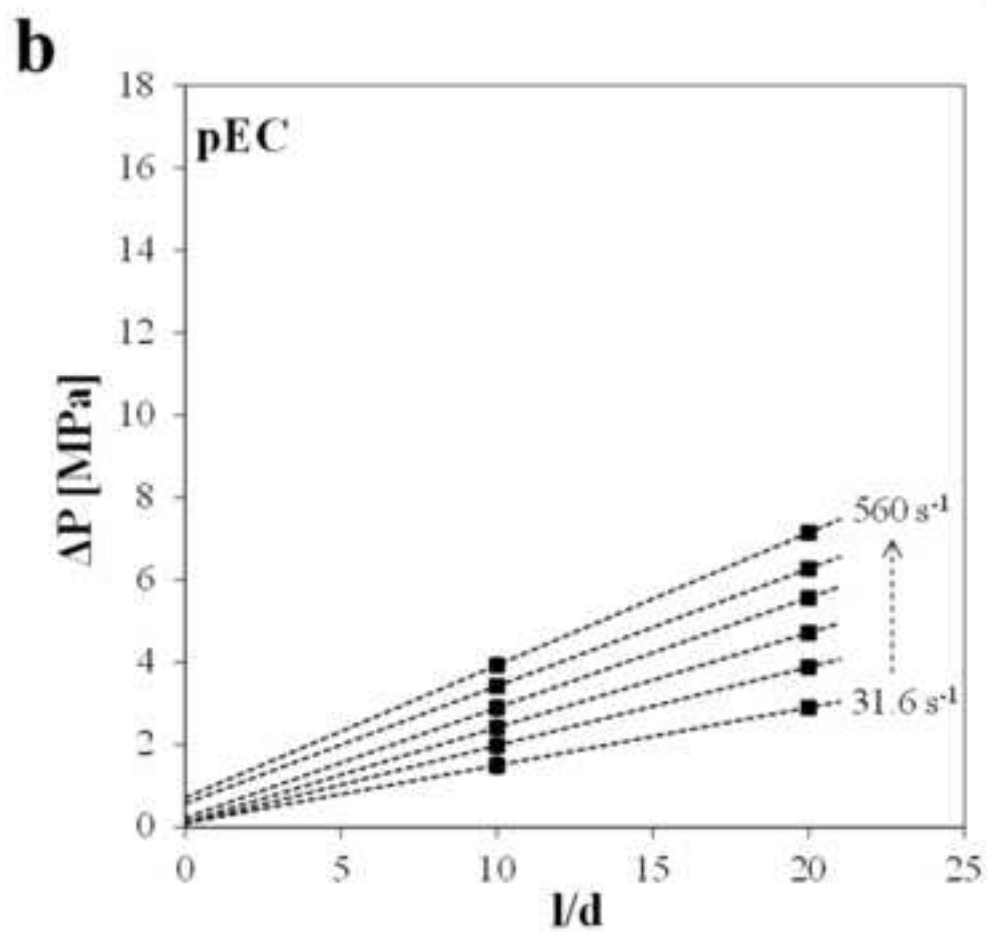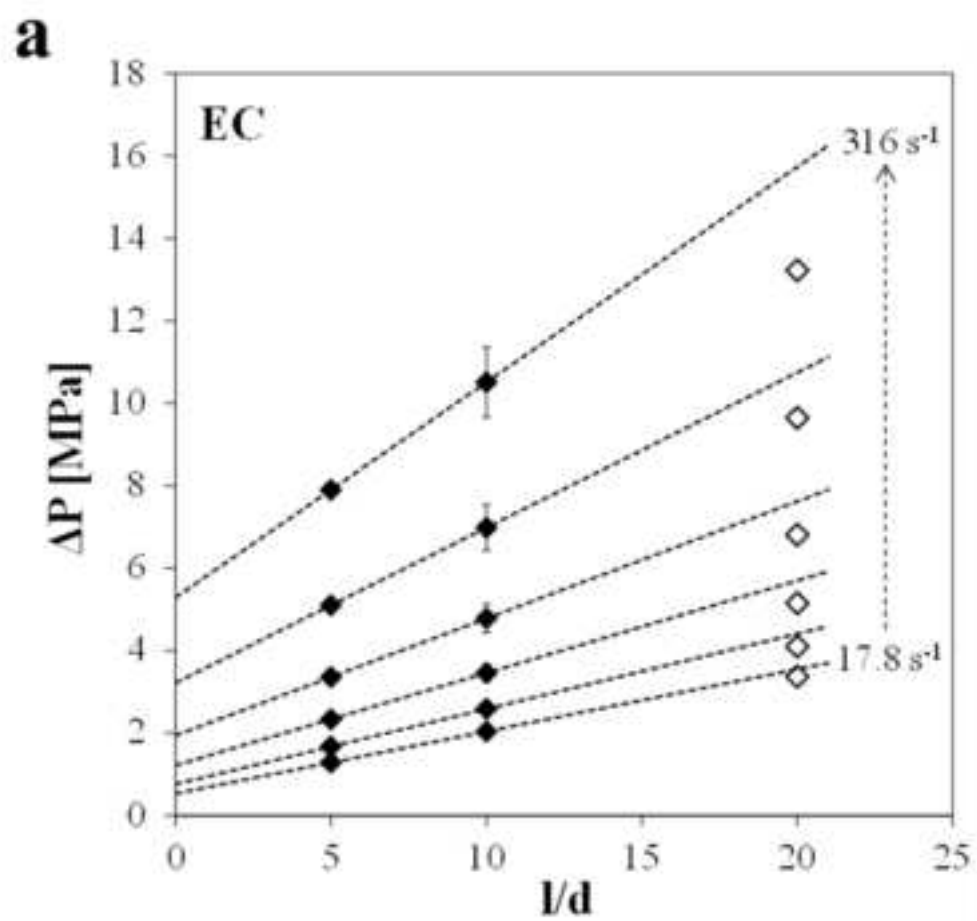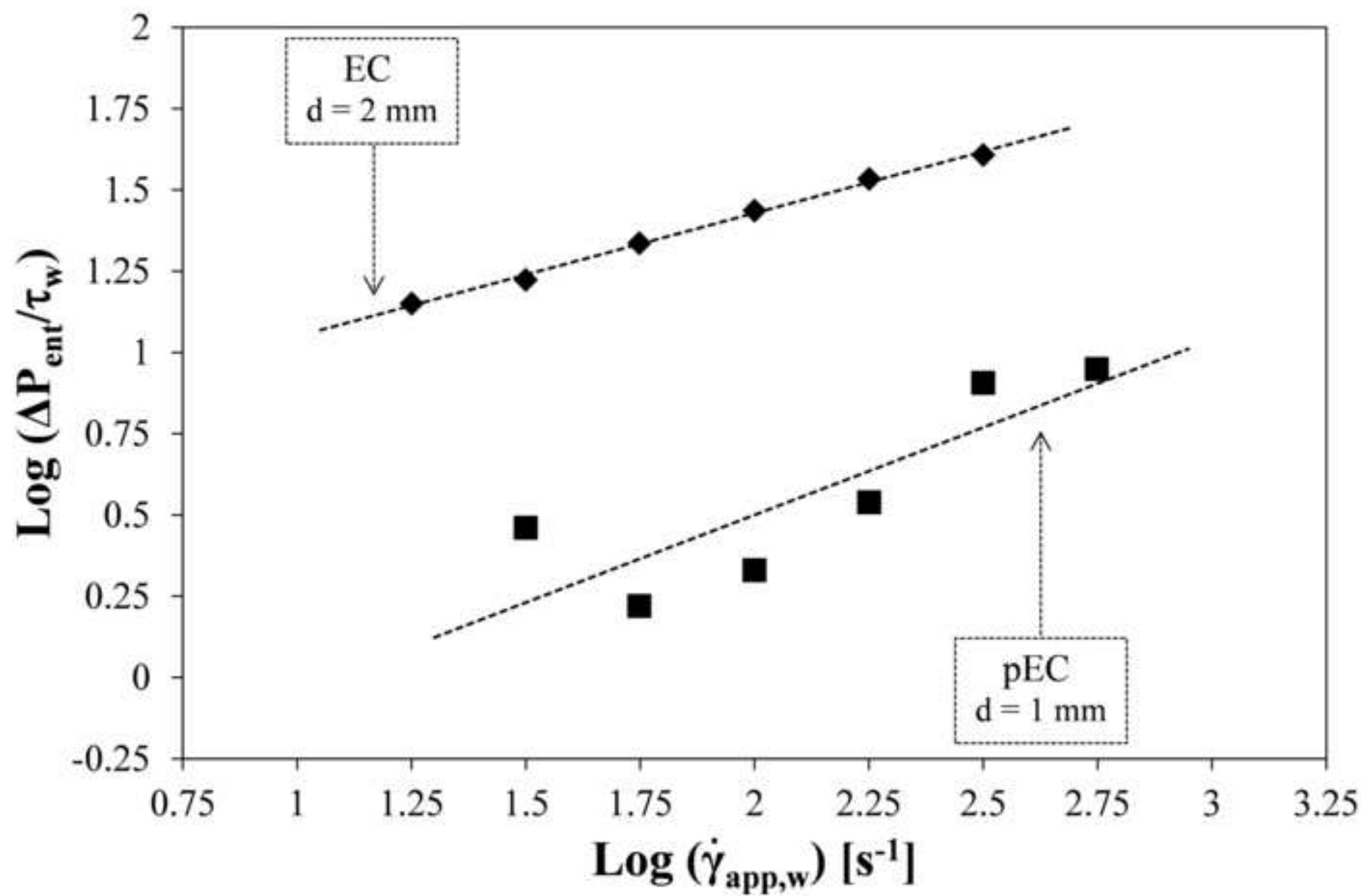
Figure 1   Click here to download Figure Fig 1 revised.tif

a

polymer melt
under analysis

V_p

P

reservoir

die

extrudate

b

M

polymer melt
under analysis

θ, ω

Figure 2

Figure 2

Figure 3

Figure 4   Click here to download Figure Fig 4 revised.tif ⬇

Figure 5

Figure 6

Figure 6

Figure 7

Click here to download Figure Fig 7 revised.tif ±

a

EC

316 s⁻¹

17.8 s⁻¹

b

pEC

560 s⁻¹

31.6 s⁻¹

Figure 8

Figure 8

Figure 9

Figure 10   Click here to download Figure Fig 10 revised.tif ⬇

Figure 10